applied optics

Magnetic-field-compensation optical vector magnetometer

Aram Papoyan,[1,*] Svetlana Shmavonyan,[1] Alen Khanbekyan,[2] Karen Khanbekyan,[3] Carmela Marinelli,[3] and Emilio Mariotti[3]

[1]Institute for Physical Research, NAS of Armenia, Ashtarak-2, 0203, Armenia
[2]Department of Physics and Earth Sciences, University of Ferrara, via Saragat 1, I-44122 Ferrara, Italy
[3]Department of Physical Sciences, Earth and Environment, University of Siena, via Roma 56, I-53100 Siena, Italy
*Corresponding author: papoyan@ipr.sci.am

Received 7 October 2015; revised 23 December 2015; accepted 23 December 2015; posted 23 December 2015 (Doc. ID 251110); published 1 February 2016

A concept for an optical magnetometer used for the measurement of magnitude and direction of a magnetic field (*B*-field) in two orthogonal directions is developed based on double scanning of a *B*-field to compensate the measured field to zero value, which is monitored by a resonant magneto-optical process in an unshielded atomic vapor cell. Implementation of the technique using the nonlinear Hanle effect on the D_2 line of rubidium demonstrates viability and efficiency of the proposed concept. The ways to enhance characteristics of the suggested technique and optimize its performance, as well as the possible extension to three-axis magnetometry, are discussed.

OCIS codes: (230.3810) Magneto-optic systems; (120.0120) Instrumentation, measurement, and metrology; (020.2930) Hyperfine structure; (280.4788) Optical sensing and sensors.

http://dx.doi.org/10.1364/AO.55.000892

1. INTRODUCTION

Optical magnetometry based on the resonant interaction of laser radiation with atomic media, notably alkali metal vapors [1,2], has gone far beyond fundamental studies, finding new applications in science, technology, and medicine. There is a variety of magneto-optical processes and experimental techniques, which can be employed to design optical magnetometers of different sensitivities and measurement ranges, including optical pumping and probing [1,3], optically detected magnetic resonance [4], spin exchange relaxation-free [5], coherent population trapping [6], electromagnetically induced transparency [7], nonlinear magneto-optical rotation [8], Zeeman and hyperfine Paschen–Back effects in nanocells [9,10], and the Hanle effect [11].

Schemes of vector magnetometers, which allow the determination of magnitude and direction of the measured field, thus extending the range of applications, are of particular interest. Several methods are employed to retrieve the vector components of the field from scalar measurements, including application of a bias field and measuring the tilt from the preferred axis [12], rotating field modulation [13], ac Stark modulation [14], and pump modulation in spin-exchange relaxation-free magnetometry [15,16].

Thanks to their remarkable performance characteristics, the state-of-the-art optical magnetometers [2] are now used for dynamical measurements of biomagnetic fields, detecting signals in NMR and MRI, inertial rotation sensing, magnetic microscopy with cold atoms, and tests of fundamental symmetries of nature. On the other hand, there are many applications in geophysics, space technologies, material science, etc., which require a large dynamic measurement range rather than remarkable sensitivity. For these applications, it is expedient to develop compact and robust devices capable of realizing unshielded vector measurements of magnetic fields in a wide range.

Techniques based on optical measurements of zero magnetic fields (compensation method) are the most appropriate for this purpose. Development of such an atomic magnetometer with autonomous frequency stabilization based on $B = 0$ resonance using polarimetric detection under excitation of a degenerate two-level system by elliptically polarized laser radiation was recently reported in [17].

Further elaborations of this concept employing other magneto-optical processes, as well as computer-controlled operations of the device including friendly readout of the measured magnetic field (*B*-field), can notably enlarge the application areas of optical magnetometers, possibly extending them also to the automated mapping applications.

In this paper, we propose yet another type of optical vector magnetometry based on the computer-controlled *B*-field compensation approach.

2. CONCEPT

The approach used in the present work is based on compensation of the actual magnetic field in the region of resonant interaction of laser radiation with atomic vapor. The vapor cell is not shielded. Instead, it is placed in an assembly of three-axis magnetic coils. A magneto-optical process used in this approach is chosen to yield a peculiarity (maximum or minimum of the recorded signal) at $B = 0$. The measurement procedure implies scanning of a magnetic field produced by the coils covering all the values in the set range of $-B_m$ to $+B_m$ with the set step. In the course of the measurement run, the scanning will pass a unique value $\vec{B}_{\text{comp}}$, at which the B-field in the interaction region is compensated to zero, so the measured value monitored by the optical signal extremum will be $\vec{B}_{\text{meas}} = -\vec{B}_{\text{comp}}$. The maximum field produced by the coils determines the maximum range of the measured B-field.

In the present work, we have used a scanning of the magnetic field along two orthogonal axes X and Y: this is provided by a simultaneous discretized linear scanning of the current in the two pairs of Helmholtz coils at different rates, as is schematically shown in Fig. 1, and the nonlinear Hanle effect under excitation by circularly polarized laser radiation directed along the Z axis [18–21] in a rubidium (Rb) vapor cell as a zero-field magneto-optical process (see below).

In the future, the setup will be modified in such a way to realize a three-component measurement making additional scanning with linearly polarized laser radiation ($\vec{E}$ along the Y axis) or by employing additional circularly polarized excitation beams directed transversely (along the Y axis), which will be sensitive to zero-compensation in the X–Z plane. Furthermore, the scanning algorithm will be optimized for the fastest determination of signal extremum coordinates by implementing "golden section search" [22] or similar algorithms. Finally, other magneto-optical processes yielding the zero B-field feature can be employed instead of the nonlinear Hanle effect.

3. EXPERIMENTAL REALIZATION AND EVALUATION OF PERFORMANCE

The schematic diagram of the experimental setup is presented in Fig. 2. It consists of two arrangements, namely, the nonlinear Hanle effect block for the fluorescence measurement [18–21]

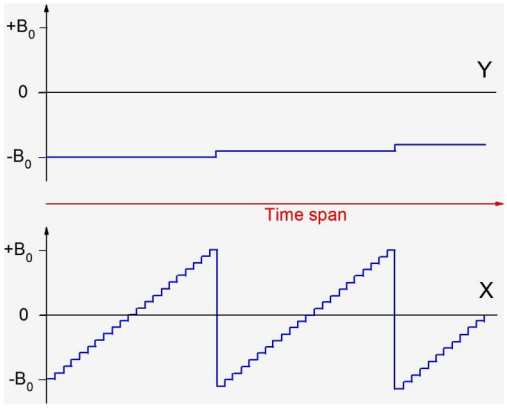

Fig. 1. Diagram of the computer-controlled scanning sequence (initial part of the run).

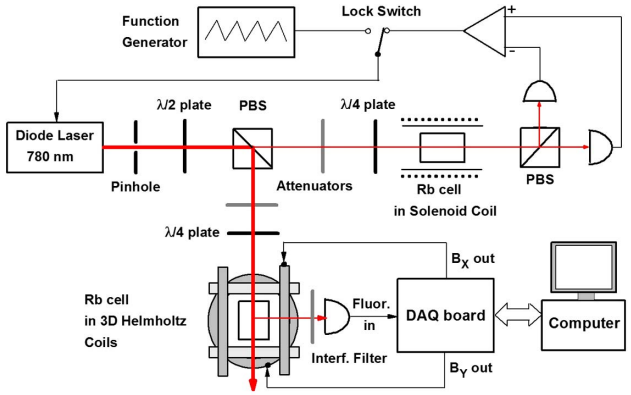

Fig. 2. Sketch of the experimental setup.

(lower part of the figure), and the dichroic atomic vapor laser locking (DAVLL) scheme [23,24] for locking the laser radiation frequency to the ^{85}Rb $F_g = 3$–$F_e = 4$ hyperfine transition of atomic D_2 line (upper right part of the figure).

The main part of radiation of a diode laser (power 35 mW, spectral linewidth 10 MHz, beam diameter 1.5 mm) was branched as a circularly polarized beam into the 5 cm long Rb vapor cell with antirelaxation polydimethylsiloxane coating. The cell was placed in the center of three pairs of mutually orthogonal calibrated Helmholtz coils providing the possibility to apply an up to ±3 G (300 μT) uniform magnetic field in the interaction region. Two pairs of coils producing a magnetic field in the X–Y plane transverse to the radiation beam were controlled by a computer via analog outputs of a PMD-1208FS USB data acquisition (DAQ) device. The third pair, producing a magnetic field in the longitudinal (Z) direction, was controlled manually to set zero magnetic field before the measurement run (in current Hanle configuration, this component of the magnetic field is the least sensitive).

A fluorescence signal emerging from the cell was recorded by a photodiode with an operational amplifier, where the output signal from which was directed to the analog input of the same DAQ device. For the ^{85}Rb $F_g = 3$–$F_e = 4$ V-type cycling hyperfine transition of the atomic D_2 line the nonlinear Hanle effect exhibits high-contrast bright resonance (increase of fluorescence) at $B_X = B_Y = 0$ [18–21]. The incident intensity of the circularly polarized laser radiation was kept on the level of 200 mW/cm^2, which is the optimum intensity to combine the high contrast of the Hanle signal with its narrow width while scanning the magnetic field.

Computer control of the B-field scanning with simultaneous recording of the fluorescence signal was realized by a code written in the LabVIEW programming environment. The screenshot of the designed user interface is shown in Fig. 3. The interface allows one to set the scanning voltage range (minimum and maximum values) and scanning step per channel (X and Y). These values determine the complete scanning time for a given DAQ device. The temporal course of scanning is monitored on the lower graphical field of the interface (black trace for X, and red trace for Y). A simultaneously recorded fluorescence signal is displayed on the upper graphical field (green trace).

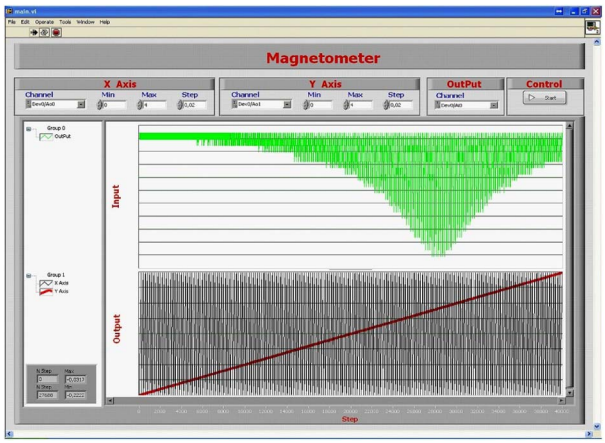

Fig. 3. Screenshot of the control interface upon completion of the typical measurement run. Horizontal scale: time. "Output" field: B-field control voltage (B_X, condensed saw line; B_Y, bold straight line). "Input" field: inverted fluorescence signal.

The output analog signal from the DAQ device was conditioned by a voltage-to-current converter, which produces the bipolar current needed to feed the Helmholtz coils. The precise current scaling for each pair of coils have been performed using an Alphalab milligauss meter (for both pairs, there was a linear response of ≈5 G/A in the region of −3 to +3 G). The same device was used to determine the compensation value for the B_Z component prior to the measurement of B_X and B_Y.

Depending on number of scanning steps (i.e., measurement precision), the complete X–Y scan lasted from 20 s (100 × 100 steps) to 10.5 min (500 × 500 steps). In order to maintain invariable laser radiation frequency throughout the measurement, the DAVLL locking scheme was used, preventing frequency jitter and drift to ≈5 MHz accuracy.

The result of a typical measurement run is presented in Fig. 4. The double scanning of a B-field (on both X and Y axes) was realized in the ±1.5 G (150 μT) range, with a step of 15 mG. With the sample rate of used DAQ device (50 kS/s), the complete run in these conditions lasts 80 s. We shall note that in spite of big scanning step, it is possible to interpolate with significantly higher precision the position of the center of the ring structure corresponding to the zero-compensation value (see lower graph in Fig. 4). Thus, the measured value is $B_X = +204$ mG; $B_Y = -581$ mG, determined with ±5 mG precision.

Let us now analyze the limitations imposed by our experimental setup and possibilities for enhancement of the magnetometer performance. Important specifications of a magnetometer are measurement range, resolution, absolute error, drift and thermal stability, sample rate, and bandwidth. We will briefly address each of these parameters.

The proposed magnetometer is based on compensation of a measured magnetic field to zero, so the measurement range is defined by the amplitude value of the scanned B-field applied to the coils. When measuring strong magnetic fields, the full-range scanning can be followed by a "zoomed" scan of the pre-identified zero region.

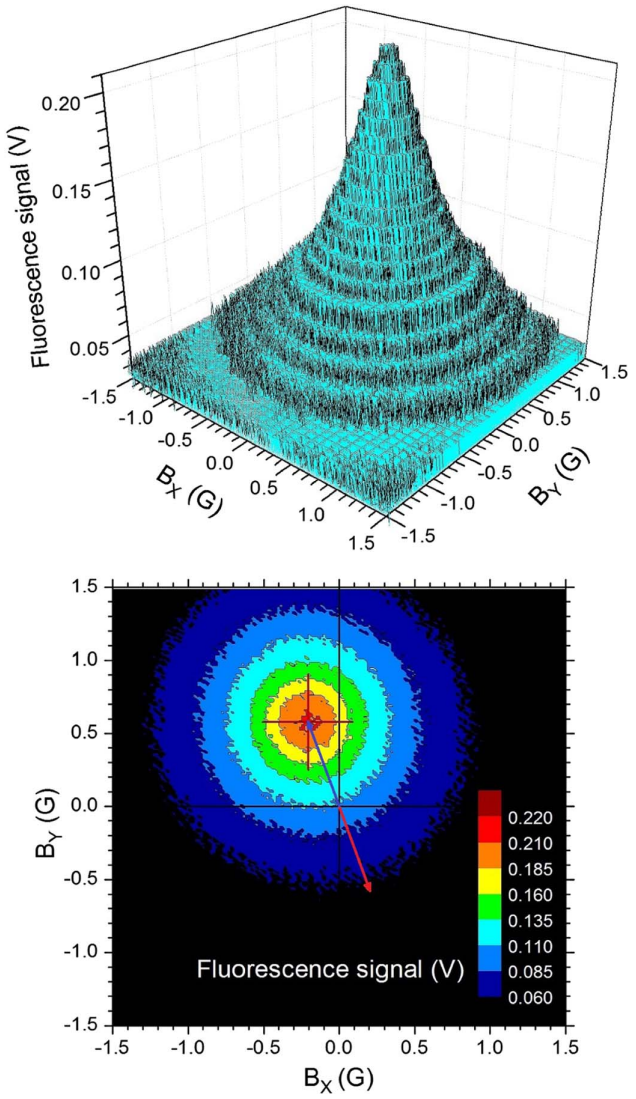

Fig. 4. Hanle fluorescence signal recorded on the ^{85}Rb $F_g = 3$–$F_e = 4$ hyperfine transition of the D_2 line while two-axis scanning (X, Y) the magnetic field in the transverse plane from −1.5 to +1.5 G. Upper graph: 3D presentation. Lower graph: color contour plot, where the center of the circular structure (red cross) corresponds to $B = 0$. The measured B-field vector in the X–Y plane ($B_X = +204$ mG; $B_Y = -581$ mG) shown by a red arrow is opposite to the compensation field (blue arrow).

As for resolution (measurement precision), it is mainly limited by a bit resolution of the DAQ device and linearity of the output voltage to coil current conversion. The resolution can be increased by decreasing the measurement step of the scanning voltage to the minimum value for given device. On the other hand, higher bit resolution for the input channel will increase the accuracy of determination of the fluorescence extremum position on the B_X – B_Y scale serving as measurement readout value (in Fig. 4, the ≈0.2 V signal was recorded just with a 10 mV step).

The issues of absolute error, drift, and thermal stability are practically not relevant for our approach, since the measured signal extremum corresponding to the compensated B-field

is linked with intrinsically stable atomic processes. Even if the fluorescence signal magnitude changes because of a thermal fluctuation or walk-off of laser radiation frequency, the signal extremum will preserve its zero-field position. The sample rate and bandwidth are mainly determined by the characteristics of the used DAQ device.

According to our estimates based on the above analysis, it is possible to reach ≈10 μG (1 nT) resolution in a single 60 s measurement run with ±5 G two-axis scanning when using a 16 bit DAQ device with a 1 MS/s sample rate.

4. CONCLUSION AND OUTLOOK

In conclusion, we proposed a concept of a two-axis optical vector magnetometer, which is based on double scanning of a B-field to find B_X and B_Y zero-compensation values, monitored by the nonlinear Hanle effect on the ^{85}Rb D_2 line in an unshielded vapor cell. The obtained ±5 mG accuracy for the ±1.5 G measurement range can be further significantly improved by the use of an appropriate data acquisition device.

As compared with other optical vector magnetometers [12–16], the proposed technique has significantly lower sensitivity and longer measurement time. Nevertheless, among its merits are simplicity and wide B-field measurement range. It can find applications for compensation of an ambient magnetic field (the B-field canceling components determined after the measurement can be applied to the same coils) for geophysical and material science studies.

Besides the above-described performance optimization, the most appropriate algorithm has to be employed in the B-field scanning control software for time-optimized steering toward an exact zero compensation value. Further development of the technique implies elaboration of the three-axis B-field measurement by exploiting also linearly polarized excitation or an additional circularly polarized laser beam directed at 90° to the initial one. Furthermore, combined with computer-controlled spatial scanning of a laser beam across the cell aperture, the technique can be extended for B-field mapping.

Funding. European Union Seventh Framework Programme (FP7/2007-2013) (295264-COSMA).

Acknowledgment. The authors are grateful to D. Sarkisyan and S. Cartaleva for stimulating discussions, to L. Stiaccini for the mechanical components realization, and to R. Cecchi for producing the electronic control units.

REFERENCES

1. D. Budker and M. Romalis, "Optical magnetometry," Nat. Phys. **3**, 227–234 (2007).
2. D. Budker and D. F. J. Kimball, eds., *Optical Magnetometry* (Cambridge University, 2013), p. 432.
3. V. Shah, S. Knappe, P. D. D. Schwindt, and J. Kitching, "Subpicotesla atomic magnetometry with a microfabricated vapour cell," Nat. Photonics **1**, 649–652 (2007).
4. A. Weis, "Optically pumped alkali magnetometers for biomedical applications," Europhys. News **43**(3), 20–23 (2012).
5. J. C. Allred, R. N. Lyman, T. W. Kornack, and M. V. Romalis, "High-sensitivity atomic magnetometer unaffected by spin-exchange relaxation," Phys. Rev. Lett. **89**, 130801 (2002).
6. P. D. D. Schwindt, S. Knappe, V. Shah, L. Hollberg, J. Kitching, L.-A. Liew, and J. Moreland, "Chip-scale atomic magnetometer," Appl. Phys. Lett. **85**, 6409–6411 (2004).
7. V. I. Yudin, A. V. Taichenachev, Y. O. Dudin, V. L. Velichansky, A. S. Zibrov, and S. A. Zibrov, "Vector magnetometry based on electromagnetically induced transparency in linearly polarized light," Phys. Rev. A **82**, 033807 (2010).
8. D. Budker, D. F. Kimball, S. M. Rochester, V. V. Yashchuk, and M. Zolotorev, "Sensitive magnetometry based on nonlinear magneto-optical rotation," Phys. Rev. A **62**, 043403 (2000).
9. A. Sargsyan, G. Hakhumyan, A. Papoyan, D. Sarkisyan, A. Atvars, and M. Auzinsh, "A novel approach to quantitative spectroscopy of atoms in a magnetic field and applications based on an atomic vapor cell with $L = \lambda$," Appl. Phys. Lett. **93**, 021119 (2008).
10. A. Sargsyan, G. Hakhumyan, C. Leroy, Y. Pashayan-Leroy, A. Papoyan, and D. Sarkisyan, "Hyperfine Paschen–Back regime realized in Rb nanocell," Opt. Lett. **37**, 1379–1381 (2012).
11. A. Kastler, "The Hanle effect and its use for the measurements of very small magnetic fields," Nucl. Instrum. Methods **110**, 259–265 (1973).
12. E. B. Alexandrov, M. V. Balabas, V. N. Kulyasov, A. E. Ivanov, A. S. Pazgalev, J. L. Rasson, A. K. Vershovski, and N. N. Yakobson, "Three-component variometer based on a scalar potassium sensor," Meas. Sci. Technol. **15**, 918–922 (2004).
13. A. K. Vershovskii, "A new method of absolute measurement of the three components of the magnetic field," Opt. Spectrosc. **101**, 309–316 (2006).
14. B. Patton, E. Zhivun, D. C. Hovde, and D. Budker, "All-optical vector atomic magnetometer," Phys. Rev. Lett. **113**, 013001 (2014).
15. S. J. Seltzer and M. V. Romalis, "Unshielded three-axis vector operation of a spin-exchange-relaxation-free atomic magnetometer," Appl. Phys. Lett. **85**, 4804–4806 (2004).
16. A. Gusarov, D. Levron, A. B.-A. Baranga, E. Paperno, and R. Shuker, "An all-optical scalar and vector spin-exchange relaxation-free magnetometer employing on-off pump modulation," J. Appl. Phys. **109**, 07E507 (2011).
17. S. Pradhan, S. Mishra, R. Behera, Poornima, and K. Dasgupta, "An atomic magnetometer with autonomous frequency stabilization and large dynamic range," Rev. Sci. Instrum. **86**, 063104 (2015).
18. Y. Dancheva, G. Alzetta, S. Cartaleva, M. Taslakov, and C. Andreeva, "Coherent effects on the Zeeman sublevels of hyperfine states in optical pumping of Rb by monomode diode laser," Opt. Commun. **178**, 103–110 (2000).
19. F. Renzoni, S. Cartaleva, G. Alzetta, and E. Arimondo, "Enhanced absorption Hanle effect in the configuration of crossed laser beam and magnetic field," Phys. Rev. A **63**, 065401 (2001).
20. A. V. Papoyan, M. Auzinsh, and K. Bergmann, "Nonlinear Hanle effect in Cs vapor under strong laser excitation," Eur. Phys. J. D **21**, 63–71 (2002).
21. A. Atvars, M. Auzinsh, E. A. Gazazyan, A. V. Papoyan, and S. V. Shmavonyan, "Implementation of a double-scanning technique for studies of the Hanle effect in rubidium vapor," Eur. Phys. J. D **44**, 411–417 (2007).
22. J. Kiefer, "Sequential minimax search for a maximum," Proc. Am. Math. Soc. **4**, 502–506 (1953).
23. K. L. Corwin, Z.-T. Lu, C. F. Hand, R. J. Epstein, and C. E. Wieman, "Frequency-stabilized diode laser with the Zeeman shift in an atomic vapor," Appl. Opt. **37**, 3295–3298 (1998).
24. V. V. Yashchuk, D. Budker, and J. R. Davis, "Laser frequency stabilization using linear magneto-optics," Rev. Sci. Instrum. **71**, 341–346 (2000).